Received: 29 April 2023 | Revised: 7 September 2023 | Accepted: 18 September 2023

IET Radar, Sonar & Navigation

DOI: 10.1049/rsn2.12480

The Institution of Engineering and Technology WILEY

ORIGINAL RESEARCH

A fast disturbance cancellation scheme for orthogonal frequency division multiplexing-based passive radar exploiting reciprocal filter

Javier Trujillo Rodriguez | **Giovanni P. Blasone** | **Fabiola Colone** | **Pierfrancesco Lombardo**

Department of Information Engineering, Electronics and Telecommunications (DIET), Sapienza University of Rome, Rome, Italy

Correspondence

Javier Trujillo Rodriguez.
Email: javier.trujillorodriguez@uniroma1.it

Abstract

This paper proposes a simple non-adaptive approach for the suppression of direct signal and clutter contributions in a passive radar system based on orthogonal frequency division multiplexing transmissions, exploiting the properties of a reciprocal filter (RF). The use of a RF allows to circumvent the limits posed by the waveform ambiguity function, producing a data-independent time-invariant response to a stationary point-like target echo at the output of the range compression stage. This feature enables simple clutter cancellation strategies, based on the subtraction of delayed portions of the surveillance signal, according to the conventional moving target indication methodologies. The proposed processing scheme consists of a range compression stage based on a RF, followed by a Single Canceller. Its performance is investigated against a simulated and an experimental data set, for the case of a digital video broadcasting-terrestial-based passive radar scenario, and it is compared to an alternative scheme based on a conventional matched filter and adaptive cancellation techniques. The proposed approach is shown to yield a perfect cancellation of the clutter returns from a stationary scene under ideal conditions. Moreover, it proves to be robust to real-world conditions, despite its considerably limited computational load compared to adaptive clutter cancellation techniques.

KEYWORDS

passive radar, radar, radar signal processing

1 | INTRODUCTION

In recent years, passive bistatic radar (PBR) systems have attracted great interest from both the scientific and industrial community. The advances in the computational capabilities and signal processing techniques have made possible the real-time implementation of long coherent integration times, a significant increase in the reliability and performance of the systems, and the successful exploitation of different existing illuminators of opportunity, [1]. Among the many available nowadays, the illuminators based on orthogonal frequency division multiplexing (OFDM) modulated waveforms represent a particularly attractive choice, due to their wide availability and useful signal properties, [2–4].

The essential signal processing stages in a PBR are the evaluation of the range-Doppler map and the suppression of the typically strong direct-path signal and clutter interference [1]. The former can be obtained by evaluating the Cross Ambiguity Function (CAF) between the surveillance signal and the reference signal, which is generally a computationally expensive task, especially in the case of wide bandwidth digital signals. As a consequence, the range-Doppler map is typically evaluated by exploiting a fast, suboptimum batching strategy, [1, 5]. In this regard, the OFDM waveforms are well suited for a batch processing architecture, as they provide an inherent fragmentation of the signals into batches, that is, the OFDM symbols [6].

Besides, the periodical OFDM signal components (pilot carriers, guard intervals, etc.) may result in an ambiguity

function characterised by undesired side-peaks and relatively high sidelobe floor, which might be responsible for ghost targets and severe masking effect on weak target echoes [4]. To overcome this issue, the use of a Reciprocal Filter (RF), in lieu of a conventional matched filter (MF) in the range compression stage, has emerged as a widely used approach, [6–11]. The RF has been shown to effectively mitigate the undesired characteristics of the signal ambiguity function, at the expense of a limited Signal-to-Noise Ratio (SNR) loss.

In addition, the application of the RF makes the response to a stationary point-like target data-independent, thus providing a time-invariant output for the range compression stage. In principle, this feature enables the application of simple clutter cancellation techniques, based on the non-adaptive subtraction of delayed portions of the surveillance signal, similar to the conventional Moving Target Indication (MTI) methodologies from pulsed active radar. This approach has been successfully exploited to enable the application of space–time clutter suppression algorithms, such as DPCA, in passive radars systems mounted on moving platforms, [8, 9].

The application of this concept was preliminary proposed in Ref. [10] for the case of a stationary PBR system. Basically, a simple scheme based on a Single Canceller (SC) approach is applied after a range compression stage exploiting a RF. Leveraging the characteristics of the RF, such a simple scheme provides an ideal cancellation of the stationary clutter, thus enabling the detection of moving targets. Furthermore, it shows some robustness even against clutter scenarios characterised by limited internal clutter motion (ICM) while tremendously limiting the computational complexity with respect to adaptive cancellation algorithms.

In this study, we extend the results in Ref. [10] by validating the performance of the RF + SC scheme against experimental data from a digital video broadcasting-terrestial (DVB-T)-based passive radar. In addition, we analyse the computational complexity of the SC and compare it with adaptive disturbance cancellation techniques typically used in OFDM radar processing.

The paper is organised as follows. The adopted signal model and processing scheme are presented in Section 2. In Section 3, the scheme is tested against simulated data, showing the key role of RF in enabling an effective clutter cancellation by means of a simple SC. Then, the comparison with a conventional adaptive cancellation algorithm is conducted in Section 4, and an analysis of the performance in the presence of ICM is performed in Section 5. In Section 6, the effectiveness of the proposed scheme is demonstrated by applying it against experimental data. Then, a comparison of the computational cost required by the SC and other conventional adaptive cancellation techniques is conducted in Section 7. Finally, our conclusions are drawn in Section 8.

2 | SIGNAL MODEL AND PROCESSING SCHEME

A passive radar system that exploits an OFDM signal of opportunity is considered. A replica of the transmitted signal, indicated as the reference signal $r[n]$, is assumed available, collected by a dedicated reference antenna pointing towards the illuminator, either used directly or after a decode/recode strategy. On the other hand, the signal received by the surveillance channel $s[n]$ includes the echoes from the area of interest.

The reference signal is written as a sequence of P OFDM symbols, each symbol being composed of N_U useful samples and a cyclical prefix (CP) of N_{CP} samples:

$$r[n] = \sum_{p=0}^{P-1} u_{N_S}[n - pN_S] \sum_{k=0}^{N_U-1} R_p[k] e^{\frac{j2\pi k(l-N_{\mathrm{CP}}-pN_S)}{N_U}} \quad (1)$$

In Equation (1), $R_p[k]$ represent the complex value transmitted at the k-th sub-carrier for the p-th OFDM symbol, whereas $u_{N_S}[n]$ is a time-windowing function of duration $N_S = N_{\mathrm{CP}} + N_U$ samples, which extends the subsequent N_U-points Discrete Fourier Transform (DFT) output over the entire OFDM symbol duration.

The evaluation of the range-Doppler map is a key processing stage for target detection [1]. Conventionally, it is performed by evaluating the Cross-Ambiguity-Function (CAF) between the surveillance signal and the reference signal. In practical situations, a direct computation of the CAF typically involves a high computational load, especially for digital signals that present a wide bandwidth. Therefore, the range-Doppler map is generally evaluated exploiting faster, suboptimal batch implementations [1, 5].

The inherent carrier orthogonality of OFDM waveforms can be exploited to obtain a favourable suboptimal implementation of the CAF, using a batching strategy here referred to as OFDM fragmentation. The batches are selected to be equal to the useful part of the OFDM symbols, after the removal of the CP encompassing N_{CP} samples. The Doppler frequency shift is neglected within each batch, which separately undergoes a range compression stage. Then, FFT is used to coherently integrate the results from the consecutive batches within the Coherent Integration Time (CIT). The obtained range-Doppler map can be expressed as

$$z[l, m] \cong \frac{1}{L} \sum_{p=0}^{P-1} w_p e^{-\frac{j2\pi mp}{P}} \sum_{k=0}^{L-1} S_p[k] H_p[k] e^{\frac{j2\pi kl}{L}} \quad (2)$$

where:

- $z[l, m]$ is the value of the Range-Doppler map at the lth range bin and mth Doppler bin;
- P is the number of OFDM symbols in the CIT;
- $S_p[k]$ is the Discrete Fourier Transform (DFT) of the pth batch of surveillance signal $s_p[n]$, at the kth sub-carrier;
- $H_p[k]$ is the range compression filter at the pth batch;
- $L = N_u$ is the number of non-zero sub-carriers in the OFDM symbol.
- w_p represents a generic spectral window.

The inner summation $\chi_p[l] = \sum_{k=0}^{L-1} S_p[k] H_p[k] e^{\frac{j2\pi kl}{L}}$ represents the range compression stage, performed in the frequency

domain. While the conventional range compression filter is the MF, which maximises the SNR at the output, the RF was introduced as an attractive mismatched solution. The RF allows to remove the side-peaks and to reduce the sidelobe floor that usually appears in the range-Doppler map due to the periodical structures included in the OFDM waveforms (e.g. pilot carriers) and to its information content [6]. This is obtained at the expense of a limited and predictable loss compared to the MF case, which depends on the used data constellation [8]. The corresponding filter coefficients in the frequency domain are specified as

$$H_p[k] = \begin{cases} R_p^*[k] & \text{MF} \\ \dfrac{1}{R_p[k]} & \text{RF} \end{cases} \tag{3}$$

In this study, we capitalise on an additional feature of the RF, which is its ability to make the signal at the output of the range compression stage data-independent. The removal of the temporal variability in the compressed radar signal batches provided by the RF can be exploited to enable simple and cost-effective disturbance cancellation strategies. This feature was proven fundamental to enable an effective clutter suppression through a non-adaptive DPCA approach for passive radars mounted on moving platforms [9], where properly delayed portions of the received signal are subtracted. In this study, an analogous concept is applied to the case of stationary passive radar.

Let us consider a scenario with N_C stationary clutter scatterers and N_T targets. The DFT of the surveillance signal at the pth batch, namely the pth OFDM symbol, can be modelled as:

$$S_p[k] = \sum_{i=0}^{N_C-1} \alpha_i R_p[k] e^{\frac{-j2\pi k l_i}{L}} + \sum_{t=0}^{N_T-1} \beta_t R_p[k] e^{-\frac{j2\pi k l_t}{L}} e^{\frac{j2\pi p m_t}{P}} + \Theta_p[k] \tag{4}$$

where the first, second, and third terms account for the clutter, target, and noise contributions, respectively. Specifically, l_i and α_i represent the range bin and complex amplitude of the ith clutter scatterer, respectively. Similarly, l_t, m_t and β_t denote the range bin, Doppler bin, and complex amplitude of the tth target, respectively. Finally, $\Theta_p[k]$ represents the DFT of an additive white Gaussian noise signal. The signal model in (4) assumes that the Doppler-induced phase shift for a given scatterer within each batch is negligible and that the maximum delay for scatterer echoes is smaller than the cyclical prefix of the OFDM symbol so that a circular shift nicely represents the delayed signal.

Using (3) and (4), the range compressed signal for both MF and RF can be obtained as

$$\begin{aligned} \chi_p^{\text{MF}}[l] = &\sum_{k=0}^{L-1} \sum_{i=0}^{N_C-1} \alpha_i \left|R_p[k]\right|^2 e^{\frac{j2\pi k(l-l_i)}{L}} \\ &+ \sum_{k=0}^{L-1} \sum_{t=0}^{N_T-1} \beta_t \left|R_p[k]\right|^2 e^{\frac{j2\pi k(l-l_t)}{L}} e^{\frac{j2\pi p m_t}{P}} + \sum_{k=0}^{L-1} \Theta_p[k] R_p^*[k] e^{\frac{j2\pi k l}{L}} \end{aligned} \tag{5}$$

$$\begin{aligned} \chi_p^{\text{RF}}[l] = &\sum_{k=0}^{L-1} \sum_{i=0}^{N_C-1} \alpha_i e^{\frac{j2\pi k(l-l_i)}{L}} + \sum_{k=0}^{L-1} \sum_{t=0}^{N_T-1} \beta_t e^{\frac{j2\pi k(l-l_t)}{L}} e^{\frac{j2\pi p m_t}{P}} \\ &+ \sum_{k=0}^{L-1} \frac{\Theta_p[k]}{R_p[k]} e^{\frac{j2\pi k l}{L}} \end{aligned} \tag{6}$$

As it is evident, the range compressed signal at the output of the MF depends on the data content $R_p[k]$. Conversely, the RF removes this dependency for the clutter and target contribution. Consequently, the clutter term in $\chi_p^{\text{RF}}[l]$ is independent of p.

As a result, the application of the RF enables the use of a simple clutter cancellation scheme based on the non-adaptive subtraction of delayed portions of the signal at the output of the range compression stage. By denoting as $\chi_{p-d}[l]$ the range compressed signal delayed by d symbols, the clutter cancellation is obtained as

$$\chi_p^{\text{SC}}[l] = \chi_p[l] - \chi_{p-d}[l] \tag{7}$$

For the sake of clarity, Figure 1 shows a diagram of the resulting processing scheme. This method resembles the Single Canceller (SC) typically used for disturbance removal in Moving Target Indication (MTI) radar systems based on the transmission of a train of identical pulses.

As for MTI systems, the amount of delay, namely the number of symbols d, determines the width of the SC cancellation notch. A high value of d produces a narrow notch at zero Doppler frequency, while lower values increase it. This dependence is illustrated in Figure 2, which shows the magnitude of the frequency response of the SC for multiple values of delay. Of course, by increasing d, the appearance of blind velocities, that could affect the detection of targets lying in the vicinity of the corresponding frequency values, must be taken into account. The separation between them clearly

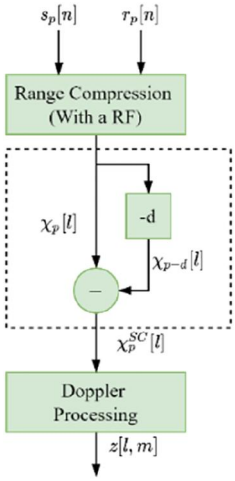

FIGURE 1 Sketch of the reciprocal filter (RF) + Single Canceller (SC) scheme.

depends on $1/d$ in normalised Doppler frequency. This is a well-known limitation of the polynomial cancellers, which sets a constraint on the design of an arbitrarily narrow cancellation notch. The setting could be properly adapted according to the specific surveillance application.

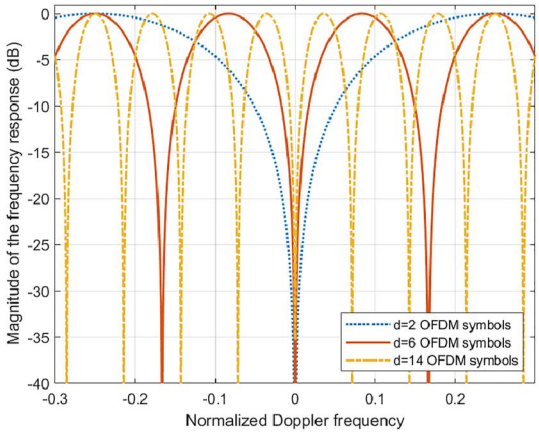

FIGURE 2 Single Canceller (SC) frequency response for multiple delay values.

3 | TEST AGAINST SIMULATED DATA

To verify the effectiveness of the proposed scheme, we tested it against a simulated data set, considering a DVB-T 8k signal modulated with a 16QAM constellation as a reference signal. Figure 3 exhibits the resulting range-Doppler maps.

A strong return at zero bistatic range and zero Doppler frequency was simulated, representing the direct signal interference, together with stationary clutter echoes. The level of direct signal contribution is set so as to control the desired direct signal-to-noise ratio (DNR). The clutter contribution is simulated as the superposition of echoes from a large number of point-like stationary scatterers uniformly arranged over a range/angle grid that spans the area around the receiver extending up to 8 km bistatic range. Specifically,

$$c[n] = \sum_{m=1}^{M_C} \gamma_m r[n - \overline{n}_m] \tag{8}$$

where $\overline{n}_m$ is the delay associated to the mth clutter scatterer, and the amplitudes γ_m ($m = 1, \ldots, M_C$) of the clutter scatterers are assumed independent and identically distributed zero-mean complex Gaussian variables, constant during the CIT. Their variance is set so as to control the overall clutter power, that is,

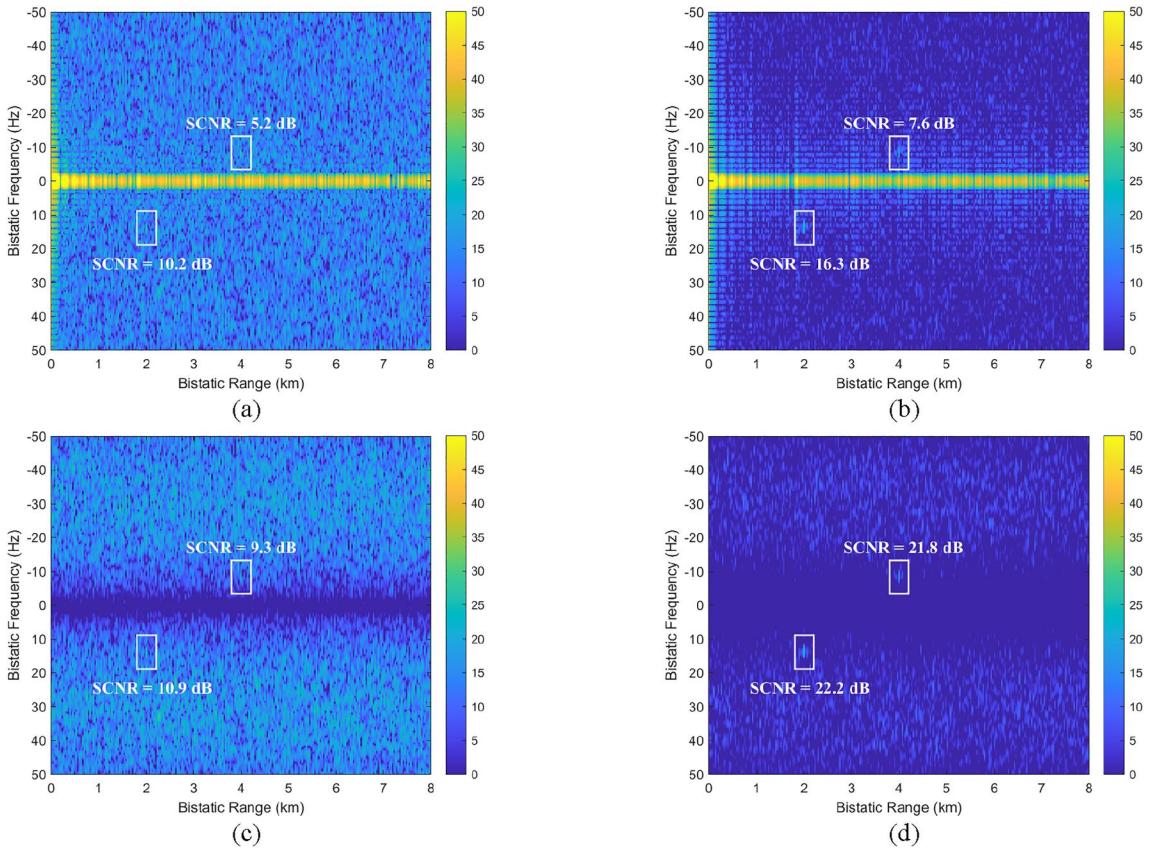

FIGURE 3 Range-Doppler maps obtained after (a) matched filter (MF), (b) reciprocal filter (RF), (c) MF with Single Canceller (SC), (d) RF with SC, for a simulated digital video broadcasting-terrestial (DVB-T) signal with stationary clutter, a point-like moving target and white noise.

$P_c = E\{|c[n]|^2\}$, and hence to simulate the desired clutter-to-noise ratio (CNR).

The simulated signal also includes two point-like moving targets, at 2 and 4 km bistatic range and 12 Hz and −9 Hz bistatic Doppler frequency, respectively.

Finally, additive white Gaussian noise was added to the signal.

Table 1 shows the DNR, CNR, and target SNR values for the simulated scenario.

Figures 3a,b show the maps resulting from the application of the MF and RF, respectively, without any clutter cancellation stage. In contrast, Figures 3c,d display the corresponding maps obtained when a SC is applied according to the scheme in Figure 1, with a delay of $d = 14$ symbols, which provides an approximate notch periodicity of 64 Hz. All figures have been scaled to the noise power level, for comparison purposes, and oversampled, to better appreciate the role played by the filters and the cancellation stage. A Taylor window is applied in the Doppler frequency dimension to keep the sidelobes level at −30 dB relative to the main peak. The resulting target Signal-to-Clutter-plus-Noise Ratio (SCNR) value has been included in each map. The disturbance power was estimated by averaging over an area surrounding the target peak, indicated by a rectangular white box.

By observing Figure 3a, we can observe that, when the MF is applied, the relatively high level of random clutter sidelobes (approximately 15 dB over the noise level) can easily mask potential moving targets. Conversely, the RF achieves a significant reduction of the random sidelobe floor (approximately 6 dB over the noise level), as visible in Figure 3b. Due to the oversampling, the deterministic sidelobes of the zero Doppler clutter contributions are visible, whose sinc shape is controlled by the tapering function. The SCNR of the slower target is largely masked by these sidelobes, while the target at 12 Hz bistatic frequency can be easily detected against the background.

After applying the SC, both Figures 3c,d show a clear cancellation of the clutter returns in the vicinity of the zero Doppler bin. However, the random sidelobe level remains at similar levels (at approximately 15 and 6 dB over the noise level). Specifically, when SC is applied in combination with the MF, it fails to effectively remove the clutter components that contribute to the random sidelobe floor, since their response is not constant over time and dependent on the data content, as seen in (5). For a numerical evaluation of the residual disturbance floor, the reader is referred to Ref. [9]. Conversely, when the SC is applied after the RF in Figure 3d, the cancellation of the clutter contributions is much more effective, thanks to the normalisation of the response with respect to (w.r.t) the waveform variability. Specifically, the deterministic sidelobe structure visible in Figure 3b is removed, leaving all the bistatic Range Doppler map at the level of the far residual sidelobes. We also observe that, under ideal conditions, a perfect removal of all the clutter contributions is achieved, resulting in a significantly higher SCNR for the considered moving targets.

TABLE 1 Parameters for the simulated scenario.

Parameter	Value
Direct signal-to-noise ratio (DNR)	20 dB
Clutter-to-noise ratio (CNR)	0 dB
Signal-to-Noise Ratio (SNR)	−40 dB

4 | COMPARISON WITH CONVENTIONAL APPROACHES

To further investigate the performance of the RF + SC scheme, we conducted a comparison against a conventional signal processing scheme commonly adopted in PBR. Specifically, such scheme exploits an adaptive clutter cancellation technique followed by the evaluation of the CAF; the latter is obtained based on (1), namely through a cascade of a MF-based range compression stage applied at batch level and a Doppler processing stage applied across batches. In PBR, adaptive techniques from the family of Extended Cancelation Algorithm (ECA) algorithms have proven to be effective and robust solutions to remove the clutter and direct signal contributions [12]. For the case of OFDM waveforms, a modified version of the ECA has been proposed, referred to as the ECA-Carriers (ECA-C) [13]. It operates by performing the ECA on a sub-carrier basis, exploiting the OFDM signal structure, which significantly reduces the required computational cost compared to the original ECA. Moreover, the ECA-C computational cost can be further reduced by leveraging an alternative processing architecture that exploits the properties of the RF [15]. However, since in this article we compare different schemes involving both MF and RF, the original ECA-C implementation is considered.

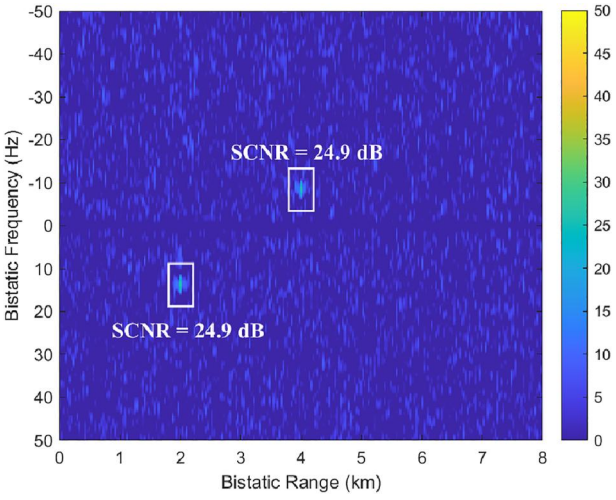

FIGURE 4 Range-Doppler map obtained after ECA-Carriers (ECA-C) with matched filter (MF), for a simulated digital video broadcasting-terrestial (DVB-T) signal with stationary clutter, a point-like moving target and white noise.

Figure 4 shows the range-Doppler map resulting from the application of the ECA-C followed by a MF to the same simulated scenario considered in Figure 3. The ECA-C algorithm adaptively projects the surveillance signal into a subspace orthogonal to the disturbance subspace. As expected, this allows not only to achieve an effective cancellation of the clutter at zero Doppler bin but also to significantly reduce the disturbance floor, compared to the case of a MF with SC (see Figure 3c). As a result, the targets in Figure 4 are clearly visible with high SCNR values.

To compare the performance of the considered signal processing schemes, Figure 5 shows the resulting target SCNR as a function of the Clutter-to-Noise Ratio (CNR) measured at the input of the overall processing chain. The ECA-C applied with the MF is compared with the SC operating after the MF and the RF. It is worth mentioning that the disturbance floor is the result of the clutter sidelobes plus noise. Therefore, low values of input CNR result in a disturbance floor dominated by noise, while high values of input CNR result in a disturbance floor where the clutter sidelobes are the main contribution.

From Figure 5, we observe that, for low input CNR values, the schemes that employ the MF for the range compression, namely the MF + SC and the ECA-C + MF, yield the highest SCNR. This is expected since the MF maximises the SNR at the output of the range compression stage. Therefore, it provides better performance, compared with the RF, in noise-limited scenarios. As the input CNR increases and the clutter returns and sidelobes contribute more to the disturbance power level, the performance of the MF + SC scheme starts decreasing, since it fails to effectively remove the clutter contribution. Conversely, the performance of the RF + SC and ECA-C + MF are not affected by the CNR increase, since both completely cancel the clutter. The difference in the final SCNR between them is only related to the adopted range compression filter. Specifically, a loss of about 2.8 dB is present, which is the expected SNR loss to be accepted when the RF is used in lieu of the MF, for a 16QAM OFDM signal, [8].

The previous results show that the ECA-C + MF scheme yields slightly better performance compared to RF + SC. However, the SC scheme involves a significantly lower computational load compared to the ECA-C algorithm, as it achieves cancellation by simply delaying the signal and performing a non-adaptive subtraction (7). On the other hand, the ECA-C involves a number of complex multiplications to adaptively estimate the filter cancellation coefficients [13]. As a result, according to our simulation environment, the SC required about 7 times less computation time than the ECA-C. This certainly represents an essential advantage, especially when considering an implementation on extremely low-cost digital hardware.

To complete the analysis, it is worth observing that the clutter cancellation based on SC heavily relies on the effectiveness of the RF in equalising the signal spectrum at the range compression stage. In other words, a non-perfect reference signal reconstruction or the use of a noisy reference signal in the absence of a demod/remod scheme might degrade the RF implementation and in turn the cancellation performance of the SC. To analyse this effect, Figure 6 shows the resulting target SCNR as a function of the SNR measured at the input of the reference channel for different processing schemes.

As apparent, all schemes show a significant SCNR degradation for low reference channel SNR values. This is expected since the reference signal quality has a non-negligible impact on both the range compression stage, either based on the MF or the RF, and the adaptive ECA-C. For reference SNR lower than 15 dB, the RF + SC scheme shows the worst degradation since the RF range compression is less robust to noisy reference signals and this in turn jeopardises the effectiveness of the SC in clutter cancellation.

Nevertheless, for reference channel SNR values above 15 dB, the gap in SCNR between ECA-C + MF and RF + SC is only due to the well-known SNR degradation caused by RF range compression (~3 dB for 16QAM). In other words, for reference channel values of SNR above 15 dB, the two approaches show the same sensitivity to the

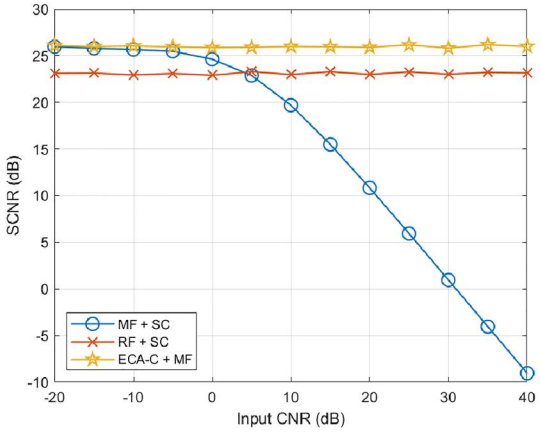

FIGURE 5 Output target Signal-to-Clutter-plus-Noise Ratio (SCNR) as a function of the input clutter-to-noise ratio (CNR), comparison between matched filter (MF)/reciprocal filter (RF) + Single Canceller (SC) approach and conventional ECA-Carriers (ECA-C) + MF scheme.

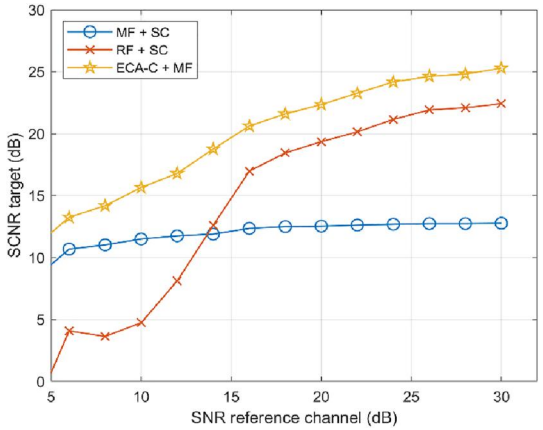

FIGURE 6 Output target Signal-to-Clutter-plus-Noise Ratio (SCNR) as a function of the reference channel Signal-to-Noise Ratio (SNR) for an input clutter-to-noise ratio (CNR) of 20 dB.

reference signal quality so that the considerations about the comparative analysis of the proposed scheme and conventional approaches still hold.

5 | EVALUATION AGAINST CLUTTER WITH ICM

We proceed with the analysis of the RF + SC scheme by testing it under non-ideal conditions and comparing its performance against conventional signal processing scheme employing adaptive cancellation techniques based on ECA, in the presence of disturbance affected by ICM. This is simulated by varying with time within the CIT of the random amplitudes of the clutter scatterers in (8), that is, $\gamma_m = \gamma_m[n]$ ($m = 1, \ldots, M_C$). To this purpose, we consider a Gaussian model for the corresponding autocorrelation coefficient:

$$\rho[n] = \exp\left[-2\pi^2\left(\frac{\sigma_v}{\lambda f_s}\right)^2 n^2\right] \tag{9}$$

where λ is the wavelength, f_s is the sampling frequency, and σ_v defines the resulting clutter spectral width.

For a fair comparison, we also include the ECA-C and Doppler shift (ECA-CD) algorithm [14], which allows to widen the filter notch of the ECA-C by expanding the clutter subspace on Doppler-shifted replicas of the reference carrier. As a result, the ECA-CD presents an improved capability to suppress disturbances with ICM compared to the ECA-C.

Figure 7 shows the range-Doppler maps obtained by applying the different processing schemes against the same scenario considered in Figure 3, with the difference that in this case the clutter is no longer ideally stationary within the CIT but characterised by an ICM modelled with a Gaussian power spectrum. The assumed RMS spectral width is $\sigma_v = 0.1$ m/s and $\sigma_v = 0.3$ m/s, respectively for the maps in the first row (1*) and in the second row (2*). The (*a), (*b), (*c), and (*d) columns indicate the applied processing scheme: RF with no cancellation (*a), RF + SC (*b), ECA-C + MF (*c), and ECA-CD + MF (*d), respectively.

In the presence of ICM, the clutter removal strongly depends on the specific position of the bistatic Range-Doppler map, and reporting specific values for a few positions would not be meaningful. Therefore, we resort to a visual analysis of the maps and we focus the performance analysis on the SCNR for the selected pair of targets. As evident from Figures 7 (1a) and (2a), there is a higher clutter spread compared to the case of no ICM in Figure 3b. In particular, in Figure 7 (2a), the highest clutter level around zero Doppler frequency, due to a wider clutter spectral width, severely degrades the SCNR of the slower target. Conversely, the SCNR of the faster target remains unchanged, compared to the case of no ICM, since the RF still effectively reduces the random sidelobe floor.

Figures 7 (1b) and (2b) show a significant reduction of the clutter power, after applying the SC. However, the targets SCNR is slightly worse compared to the case of no ICM shown in Figure 3d. This is expected, since the cancellation capability of the SC is reduced by the temporal variability of the clutter disturbance. As a result, the map in Figure 7 (2b) shows lower SCNR values, especially for the slower target. Nevertheless, by comparing the maps on the first and second column, it is evident that applying the SC still provides a significant improvement in the SCNR (compared to a processing scheme without cancellation), even in the case of a wide RMS ICM.

Similarly, Figure 7 (1c) and (2c) shows that the ECA-C + MF improves the target SCNR, but its effectiveness is drastically reduced compared to the case of no ICM shown in

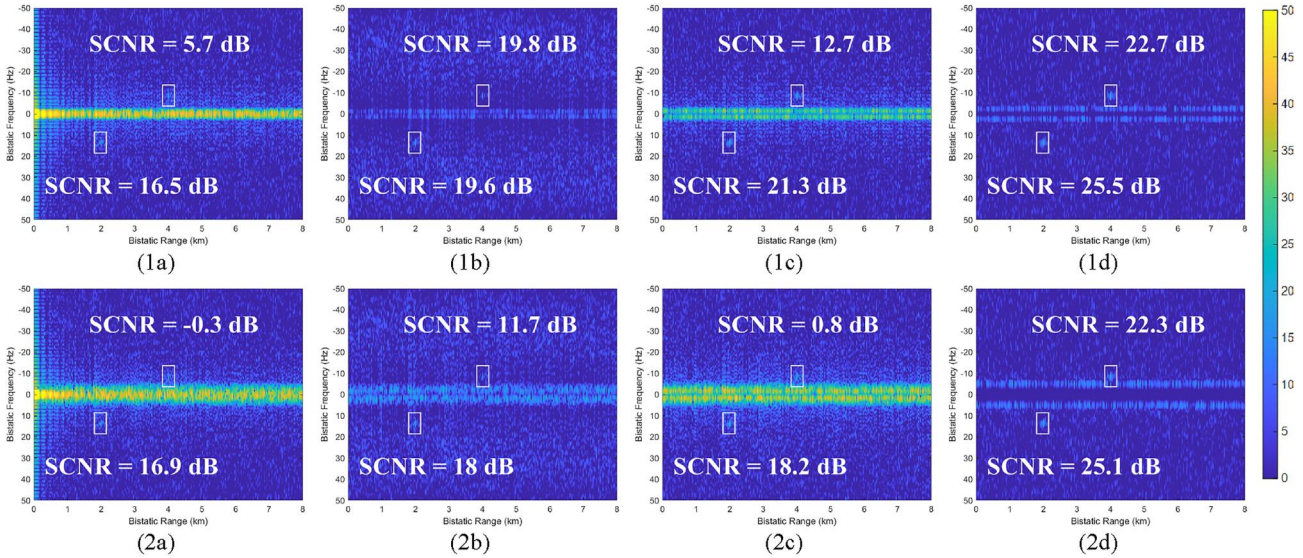

FIGURE 7 Range-Doppler maps obtained after (*a) reciprocal filter (RF) (*b) RF + Single Canceller (SC) (*c) ECA-Carriers (ECA-C) + matched filter (MF) (*d) ECA-C and Doppler shift (ECA-CD) + MF for a digital video broadcasting-terrestial (DVB-T) signal with two point-like moving targets, white noise and internal clutter motion (ICM) Gaussian clutter with (1*) $\sigma_v = 0.1$ m/s and (2*) $\sigma_v = 0.3$ m/s.

Figure 4. As expected, the filter adaptively suppresses the clutter at zero Doppler bin while it fails to remove the Doppler-spread clutter returns.

Moreover, the clutter residuals around zero Doppler frequency are much higher than the RF + SC case, resulting in a significant SCNR degradation for the slower target, especially in the case of $\sigma_v = 0.3$ m/s.

Finally, Figures 7 (1d) and (2d) show the highest SCNR for both targets since the ECA-CD effectively removes the Doppler-spread clutter. To achieve this, the algorithm requires several complex matrix multiplications and inversions to adaptively estimate the cancellation filter coefficients. This greatly increases its computational load compared to the ECA-C. In contrast, the SC represents a considerably faster non-adaptive approach and, although it shows a reduced performance in the presence of ICM, it is still able to provide final SCNR values that are only moderately lower than the ECA-CD case.

6 | EVALUATION AGAINST EXPERIMENTAL DATA

The performance of the proposed RF + SC scheme was also tested against an experimental data set, collected by a passive receiver exploiting a DVB-T transmitter as the illuminator of opportunity. The acquisition was performed along the shore of Civitavecchia (about 70 km North of Rome), with a passive radar receiver from the Radar and Remote Sensing Group of Sapienza University of Rome.

The experimental setup is depicted in Figure 8. The receiver gathered an 8K DVB-T signal from a transmitter, located at about 4.4 km from the receiver, through a dedicated reference channel. In addition, a surveillance channel was steered to the open sea with the purpose of detecting potential maritime targets. In addition, a small cooperative boat, which is shown in Figure 9, performed a predefined trajectory. Table 2 shows the signal and processing parameters of the experimental test.

The processing steps can be described as follows. First, in a pre-processing stage, we identified the OFDM frame start and used it for synchronising the surveillance and reference signal. Then, the signals were divided into 120 CITs of 1.5 s duration and fed into a processing chain that evaluates the range-Doppler map for each CIT and removes the disturbance. Obviously, the specific algorithms and order of the processing stages depend on the considered processing scheme (e.g. RF + SC, ECA-C + MF). Finally, targets are detected using a square-law Cell Average CFAR (CA-CFAR) detector.

The range-velocity maps obtained for all the considered schemes when applied to a single CIT are shown in Figure 10. Two targets of opportunity, with low and high velocity, are of interest in the resulting maps and their SCNR values have been explicitly reported in each figure. The disturbance power was estimated by averaging over an area surrounding the target peak, indicated by a rectangular white box around each target.

The disturbance contribution can be clearly seen in Figures 10a,b, which exhibit the range-velocity maps obtained when respectively the MF and RF are applied for range compression, without any disturbance cancellation algorithm. As visible, the strongest clutter echoes appear at zero Doppler velocity and close bistatic ranges below 1 km. In addition, at those ranges, a small clutter ICM is observed, spreading to a few Doppler bins around zero velocity. On the other hand, for bistatic ranges above 1 km, the clutter is weaker and its contribution is limited to the zero Doppler bin. As expected, since the disturbance is not removed, the SCNR values obtained for the slow target significantly impacted for both the MF and RF. On the other hand, the

FIGURE 8 Setup for the experimental data acquisition.

FIGURE 9 Small cooperative boat.

TABLE 2 Parameters of the experimental test.

Symbol	Description	Value
DVB-T signal parameters		
f_c	Carrier frequency	690 MHz
T_S	OFDM symbol duration	1100 us
T_U	Useful part duration	896 us
T_{CP}	CP duration	112 us
C	Constellation	64 QAM
Processing parameters		
T_{CIT}	Coherent integrations time	1.5 s
P_{fa}	Probability of false alarm	10^{-8}
N_{CIT}	Number of CITs analysed	120

SCNR of the fast target obtained for the RF is higher than the SCNR value resulting from the MF. This is a consequence of the higher reduction on the random sidelobe floor provided by the RF with respect to the MF, which is clearly visible when comparing the floor level of Figures 10a,b.

Figure 10c,d show the range-velocity maps obtained for the MF + SC and RF + SC respectively. As visible, the stationary clutter contribution is now removed by the SC, with a cancellation notch resulting from $d = 10$ delayed OFDM symbols with an approximate notch periodicity of 38 m/s. As a result, in both maps, the SCNR value observed for the slow target is increased compared to the corresponding range compression strategies when a disturbance cancellation stage is not implemented (see Figure 10a,b). However, the RF + SC scheme yields higher SCNR values than the MF + SC for both targets. Moreover, it is clearly visible that the MF + SC scheme fails to effectively remove the clutter random sidelobes floor. This is due to the time variability of the range-compressed signal at the output of the MF and confirms the results obtained against the simulated data. Finally, it is worth noting in Figures 10c,d that there is a slight increase in the disturbance floor for medium to high velocities compared to Figures 10a,b. This is due to the sinusoidal frequency response of the SC; however, this does not impact the SCNR since the magnitude of a target moving at those velocities is boosted by the same amount.

Finally, Figures 10e,f show the range-velocity maps obtained when using conventional signal processing schemes encompassing adaptive cancellation algorithms, namely ECA-C + MF and ECA-CD + MF. Stationary clutter is removed in both maps. However, as expected, the ECA-CD offers improved cancellation due to a wider notch, which spreads to the Doppler bins adjacent to zero velocity at $\delta v = \pm 0.14$ m/s, following [14]. This results in a higher SCNR, especially for the slow target, compared to the RF + SC.

To further compare the performance of the considered schemes, we analysed their detection performance during the 120 CITs. Figure 11 shows the stacked detections in the range-velocity map obtained when the RF + SC scheme is applied to the whole experimental data. We have marked six targets of interest with black rectangles and labelled them on the map. In

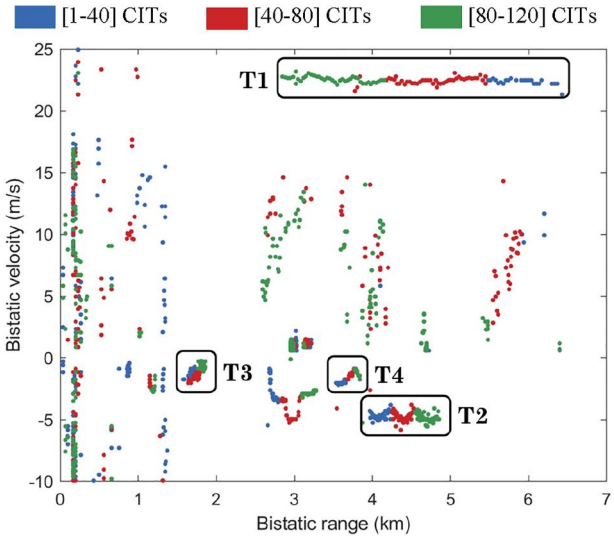

FIGURE 11 Map of all the detections obtained in 120 Coherent Integration Times (CITs) for the reciprocal filter (RF) + Single Canceller (SC) scheme applied to the experimental data.

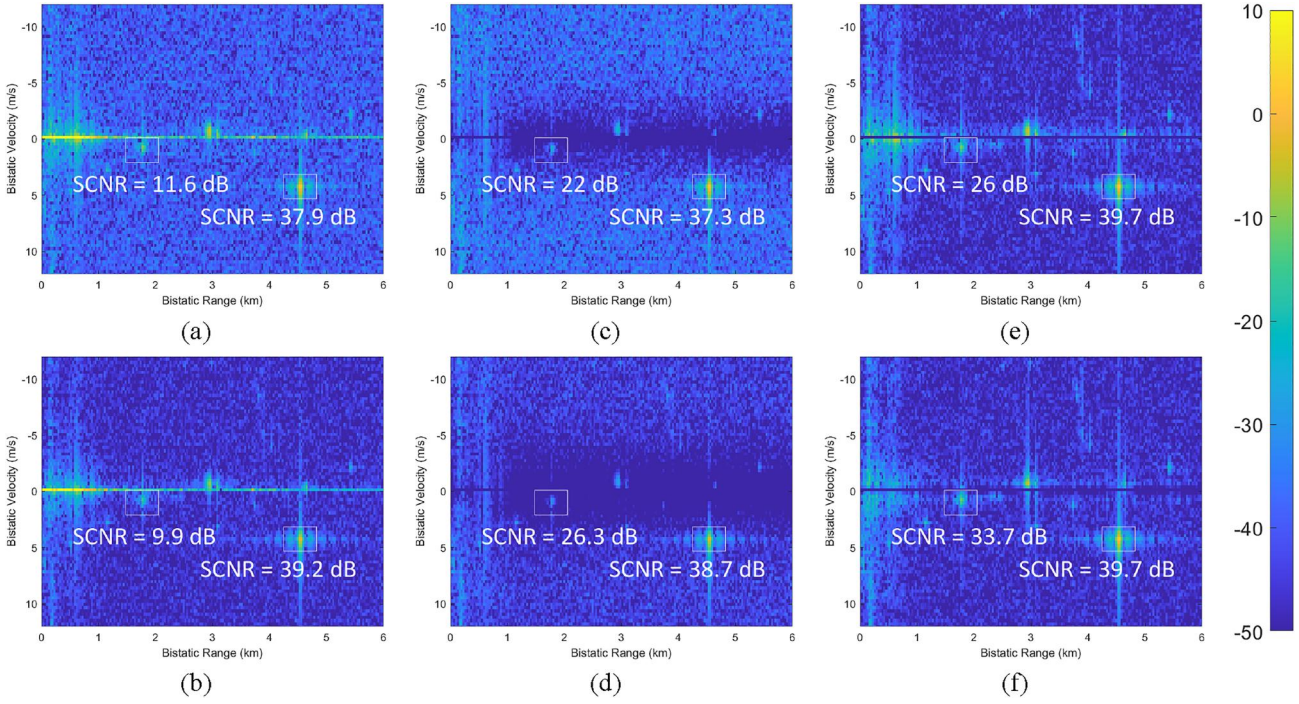

FIGURE 10 Range-velocity maps of (a) matched filter (MF), (b) reciprocal filter (RF), (c) MF + Single Canceller (SC), (d) RF + SC, (e) ECA-Carriers (ECA-C) + MF, and (f) ECA-C and Doppler shift (ECA-CD) + MF applied to a single Coherent Integration Time (CIT) of the experimental data.

addition, colours have been used to indicate the CIT range at which detections have been made; blue are detections made on the first 40 CITs, red on the middle CITs between 40 and 80, and finally green on the last 40 CITs.

It is worth mentioning that T1 represents the small cooperative boat approaching the receiver at an approximately constant bistatic velocity of 22 m/s. The other targets are vessels and boats in close bistatic ranges, moving away from the receiver at low velocities. In particular, T3 and T2 respectively correspond to the slow and fast targets appearing in the range-velocity maps of Figure 10.

Table 3 shows the number of CITs in which each target has been detected D_{CIT} using the considered processing schemes. To better understand the results, similar targets have been grouped according to their SCNR and bistatic velocity.

In particular, targets T1 and T2 are detected consistently across the acquisition time by all the processing schemes. This is because these targets produce strong echoes resulting in high SCNR values. Moreover, they move at relatively high velocities, thus their detection is not strongly affected by the clutter returns, as visible for T2 in Figure 10. Therefore, even the processing schemes without a disturbance cancellation stage, namely the MF and RF (see first two rows of Table 3), are able to detect these targets in most of the CITs. In other words, the removal of clutter does not have a significant impact on the detection performance for these targets.

In contrast, targets T3 and T4 move at slower bistatic velocity and, consequently, their detection is affected by clutter contributions generated around the zero Doppler. For this reason, the MF and RF schemes, without a disturbance cancellation stage, are unable to continuously detect these targets during the acquisition time. In this case, the addition of a clutter cancellation stage sensibly improves the detection rate with all the considered approaches.

Specifically, when using the proposed scheme based on a simple SC applied after the range compression stage, we observe that the number of correct detections across the observation time increases by a factor larger than 3 for both targets if the range compression is performed based on the RF. In contrast, the improvement reduces with the MF + SC scheme since the SC cannot rely on a time invariant range compression output so that it is not effective against the random sidelobes floor due to the clutter returns.

TABLE 3 Number of Coherent Integration Times (CITs) in which each target has been detected D_{CIT} using the different processing schemes.

	High velocity, high SCNR		Low velocity, low SCNR	
Scheme	**T1**	**T2**	**T3**	**T4**
MF	99	120	31	26
RF	101	120	23	28
MF + SC	99	120	85	79
RF + SC	101	120	90	87
ECA-C + MF	105	120	82	109
ECA-CD + MF	105	120	98	114

Note: 'Green' is used for results proving a D_{CIT} equal or greater than 80; 'yellow' is used for values of D_{CIT} between 40 and 80; 'red' is used for values of D_{CIT} smaller than 40.

The conventional ECA-C + MF and ECA-CD + MF schemes are able to provide remarkable detection performance thanks to the effectiveness of the adaptive cancellation stage and the limited range compression loss of the MF. Obviously, this is paid in terms of computational complexity as detailed in the next section. However, we observe that, at least for T3, the ECA-C + MF does not offer improved performance with respect to the proposed RF + SC. This is due to the fact that clutter contributions in the bistatic ranges of T3 are probably affected by a non-negligible ICM. As stated in Section 5, the SC is more robust against clutter ICM than the ECA-C, which results in a slightly enhanced performance despite the additional SNR loss of the RF-based range compression stage.

It is worth mentioning that the benefits of the proposed RF + SC approach in this particular dataset are somehow limited by the fact that the considered experimental scenario is not severely limited by clutter, both in terms of the clutter power level and in terms of ICM, as for the simulated case study considered in Sections 2–5. Therefore, based on the analysis of the previous sections, enhanced improvements could be expected in more severe scenarios. Furthermore, in implementing the range compression we used a non-ideal reference signal (i.e. that obtained from a dedicated antenna pointed towards the Tx of opportunity, without any reconstruction). This might yield a non-perfect equalisation by the RF and a degradation of its capability to reduce the random sidelobe floor. An analysis of the impact of a non-ideal reference signal in the range compression will be explored in future works.

Nevertheless, we observe that the straightforward RF + SC processing scheme offers comparable performance with respect to the ECA-C + MF without requiring any adaptive estimation of the relevant parameters, thus providing a much cheaper solution. Overall, the ECA-CD yields the best performance due to a combination of a wide cancellation notch with a lossless range compression based on the MF. However, as stated before, this improvement is paid in terms of a tremendous increase in terms of computational cost w.r.t the proposed approach which might not be feasible if it has to be implemented in lightweight compact PBR sensors. The comparison in terms of computational complexity is detailed in the following section.

7 | COMPUTATIONAL COST ANALYSIS

Table 4 shows the number of complex multiplications (CM) and complex additions (CA) required by the SC, ECA-C, and ECA-CD. In addition, the analytical expression of each cancellation technique has been included. The CM and CA are expressed as a function of the number of OFDM symbols P and the number of useful carriers in the OFDM symbol $L = N_u$.

From (7), the SC achieves cancellation by subtracting a d OFDM symbols delayed replica of the range-compressed signal. As a result, it does not require any complex CM and PL CA. On the other hand, the ECA-C cancellation, as defined in Ref. [13], is based on a per-carrier projection of the

surveillance signal on a subspace orthogonal to the disturbance subspace. This operation is represented in Table 4, where $\boldsymbol{S}_k$ and $\boldsymbol{R}_k$ are $P \times 1$ vectors containing the kth carrier value at each OFDM symbol. This results in an increased number of operations compared to the SC.

Finally, the ECA-CD extends the clutter subspace by considering q symmetric replicas around Doppler zero. The resulting expression is included in Table 4, being $\boldsymbol{Q}_k$ a $P \times W$ matrix with $W = 2q + 1$. As visible, the ECA-CD requires the inversion of a matrix which largely increases its computational cost with respect to the ECA-C. Obviously, this is compensated by an improved cancellation capability against ICM disturbances.

To extend the analysis, we estimated the number of floating-point operations (FLOPs) required by each cancellation technique as a function of the CIT duration. It is assumed that a CM involves 6 FLOPs, while a CA only requires 2 FLOPs.

Figure 12, shows the results obtained based on the CM and CA values of Table 4. The computational load of each algorithm has been evaluated assuming the same parameters adopted for the experimental test. Specifically, we consider the experimental DVB-T with $L = 8192$ useful carriers. In addition, the ECA-CD is set to $q = 1$ symmetric replicas which are used for the experimental test. Moreover, to aid the analysis, the considered $T_{\mathrm{CIT}} = 1.5$ s is represented with a black dashed line.

As visible from the figure, both the ECA-C and ECA-CD require a much higher number of FLOPs than the SC as a function of the CIT duration. In particular, at the considered $T_{\mathrm{CIT}} = 1.5$ s, the ECA-C requires more than 10 times the number of FLOPs than the SC. This difference is even higher for the ECA-CD, which involves around 60 times more FLOPs compared to the SC even for its most basic implementation with $q = 1$.

8 | CONCLUSIONS

In this study, we proposed a simple approach for clutter cancellation in OFDM-based passive radar systems, exploiting the properties of the RF. It was demonstrated that the RF produces a data-independent signal at the output of the range compression stage. This feature allows to implement simple subsequent clutter cancellation strategies, based on the subtraction of delayed portions of the surveillance signal.

A processing scheme was presented, encompassing a range compression stage based on RF, followed by a SC. This consists in subtracting a replica of the range-compressed signal delayed by an integer number of OFDM symbols. Under ideal conditions, a perfect cancellation of stationary clutter echoes, as well as of the direct signal interference, could be achieved.

First, the performance of the scheme was evaluated in a simulated scenario, assuming a DVB-T-based passive radar, and compared with that obtained in the case of a MF. The results showed that the SC fails to completely remove the clutter background when a MF is used, while it achieves an effective cancellation when applied after a RF. The performance of the SC was also compared with a traditional adaptive cancellation scheme, namely the ECA-C, in terms of achievable SCNR. The RF + SC scheme proved to be effective and preferable over the MF + SC, especially in the case of high CNR. Moreover, although the SC showed a slight loss compared to the ECA-C algorithm, it allows a much simpler and faster implementation.

Then, the scheme capability was tested against a disturbance affected by ICM. In this case, the cancellation performance of the SC was reduced by the temporal variability of the clutter. However, it was shown to be more robust than the ECA-C for slow targets, and almost as effective as the largely more expensive ECA-CD.

Afterwards, the results were validated by comparing the schemes performance against experimental data from a PR exploiting a DVB-T illuminator of opportunity. The results obtained were compliant with those from the simulated scenario. In particular, it was shown that, for the considered application, the RF + SC offers a detection performance comparable to the ECA-C + MF.

Finally, an extensive analysis of the computational cost and number of FLOPs required by each cancellation technique was

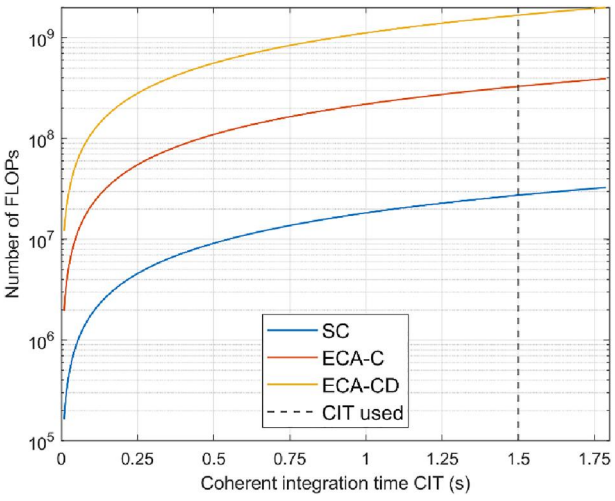

FIGURE 12 Number of floating-point operations (FLOPs) required by the Single Canceller (SC), ECA-Carriers (ECA-C) and ECA-C and Doppler shift (ECA-CD) as a function of the Coherent Integration Time (CIT) duration.

TABLE 4 Computational cost expressed in number of complex multiplications and complex additions for the Single Canceller (SC), ECA-Carriers (ECA-C), and ECA-C and Doppler shift (ECA-CD) cancellation algorithms.

Algorithm	Expression	# Complex multiplications (CM)	# Complex additions (CA)
SC	$\boldsymbol{\chi}_p - \boldsymbol{\chi}_{p-d}$	0	PL
ECA-C	$\boldsymbol{S}_k - \frac{\boldsymbol{R}_k \boldsymbol{R}_k^H}{\lvert\boldsymbol{R}_k\rvert^2}\boldsymbol{S}_k$	$3PL$	$3PL$
ECA-CD	$\boldsymbol{S}_k - \boldsymbol{Q}_k\left(\boldsymbol{Q}_k^H \boldsymbol{Q}_k\right)^{-1}\boldsymbol{Q}_k^H \boldsymbol{S}_k$	$L\left(\frac{1}{2}W^3 + \frac{5}{2}W^2 + W^2P + 2WP\right)$	$L\left(\frac{1}{2}W^3 + \frac{1}{2}W^2 + W^2P + 2WP + P\right)$

conducted. It showed that both the ECA-C and ECA-CD involve a much higher number of operations than the SC which can speed-up the cancellation stage at least by a 10x factor. Further work will investigate the design of polynomial cancellers and other cancellation techniques able to exploit the properties of a RF-based range compression.

AUTHOR CONTRIBUTIONS

Javier Trujillo Rodriguez: Software (lead); validation (lead); visualisation (lead); writing – original draft (lead); writing – review & editing (lead); formal analysis (lead). **Giovanni P. Blasone:** Software (supporting); writing – original draft (supporting); data curation (lead); writing – review & editing (supporting). **Fabiola Colone:** Conceptualisation (lead); methodology (lead); supervision (lead); resources (lead); writing – original draft (supporting); writing – review & editing (supporting). **Pierfrancesco Lombardo:** Conceptualisation (supporting); supervision (supporting); funding acquisition (lead); project administration (lead); writing – review & editing (supporting).

ACKNOWLEDGEMENTS

This work was partially supported by the European Union under the Italian National Recovery and Resilience Plan (NRRP) of NextGenerationEU, partnership on 'Telecommunications of the Future' (PE00000001 - program 'RESTART', CUP B53C22004050001).

CONFLICT OF INTEREST STATEMENT

I am aware that this journal requires all authors to disclose any potential sources of conflict of interest in the manuscript. We declare no conflict of interest to disclose.

DATA AVAILABILITY STATEMENT

The data that support the findings of this study are available from the corresponding author upon reasonable request.

ORCID

Javier Trujillo Rodriguez https://orcid.org/0000-0002-1468-6942

REFERENCES

1. Lombardo, P., Colone, F.: Advanced processing methods for passive bistatic radar systems. In: Melvin, W.L., Scheer, J.A. (eds.) Principles of Modern Radar: Advanced Radar Techniques, pp. 739–821. SciTech (2012)
2. Berger, C., et al.: Signal processing for passive radar using OFDM waveforms. IEEE J. Sel. Topics Signal Process. 4(1), 226–238 (2010). https://doi.org/10.1109/jstsp.2009.2038977
3. Palmer, J., et al.: DVB-T passive radar signal processing. IEEE Trans. Signal Process. 61(8), 2116–2126 (2013). https://doi.org/10.1109/tsp.2012.2236324
4. Colone, F., Langellotti, D., Lombardo, P.: DVB-T signal ambiguity function control for passive radars. IEEE Trans. Aero. Electron. Syst. 50(1), 329–347 (2014). https://doi.org/10.1109/taes.2013.120616
5. Moscardini, C., et al.: Batches algorithm for passive radar: a theoretical analysis. IEEE Trans. Aero. Electron. Syst. 51(2), 1475–1487 (2015). https://doi.org/10.1109/taes.2015.130407
6. Searle, S., et al.: Evaluation of the ambiguity function for passive radar with OFDM transmissions. In: 2014 IEEE Radar Conference, pp. 1040–1045 (2014)
7. Glende, M.: PCL-signal-processing for sidelobe reduction in case of periodical illuminator signals. In: Int. Radar Symposium. Krakow (2006)
8. Wojaczek, P., et al.: Reciprocal-filter-based STAP for passive radar on moving platforms. IEEE Trans. Aero. Electron. Syst. 55(2), 967–988 (2019). https://doi.org/10.1109/taes.2018.2867688
9. Blasone, G.P., et al.: Passive radar DPCA schemes with adaptive channel calibration. IEEE Trans. Aero. Electron. Syst. 56(5), 4014–4034 (2020). https://doi.org/10.1109/taes.2020.2987478
10. Trujillo Rodriguez, J., et al.: A simple clutter suppression approach for OFDM-based passive radar exploiting reciprocal filter. In: 2022 International Conference on Radar System (Radar). Edinburgh (2022)
11. Trujillo Rodriguez, J., Colone, F., Lombardo, P.: Loaded reciprocal filter for OFDM-based passive radar signal processing. In: 2022 IEEE Radar Conf. New York (2022)
12. Colone, F., et al.: A multistage processing algorithm for disturbance removal and target detection in passive bistatic radar. IEEE Trans. Aero. Electron. Syst. 45(2), 698–722 (2009). https://doi.org/10.1109/taes.2009.5089551
13. Zhao, Z., et al.: Multipath clutter rejection for digital radio mondiale-based HF passive bistatic radar with OFDM waveform. IET Radar, Sonar Navig. 6(9), 867–872 (2012). https://doi.org/10.1049/iet-rsn.2012.0011
14. Schwark, C., Cristallini, D.: Advanced multipath clutter cancellation in OFDM-based passive radar systems. In: 2016 IEEE Radar Conference, pp. 1–4 (2016)
15. Trujillo Rodriguez, J., Colone, F., Lombardo, P.: Supervised reciprocal filter for OFDM radar signal processing. IEEE Trans. Aero. Electron. Syst. 59(4), 3871–3889 (2023). https://doi.org/10.1109/TAES.2023.3235317

How to cite this article: Trujillo Rodriguez, J., et al.: A fast disturbance cancellation scheme for orthogonal frequency division multiplexing-based passive radar exploiting reciprocal filter. IET Radar Sonar Navig. 18(1), 56–67 (2024). https://doi.org/10.1049/rsn2.12480